Research Square

Preprints are preliminary reports that have not undergone peer review.
They should not be considered conclusive, used to inform clinical practice,
or referenced by the media as validated information.

Chromosome-level genome reveals the phylogenomics and hibernation-related evolution in Tibetan brown bear (Ursus arctos pruinosus)

Muran Zhao
Qinghai Normal University
Anmin Wang
Qinghai Normal University
Hai Liu
Qinghai Normal University
Chenxing Yu
Qinghai Normal University
Yanlin Liu
Qinghai Normal University
Nan Sun
Qinghai Normal University
Guogang Li
qhnulgg@126.com
Qinghai Normal University

Research Article

Keywords: Chromosome-level genome, De novo assembly, Tibetan brown bear, Hibernation adaptation

Posted Date: July 31st, 2026

DOI: https://doi.org/10.21203/rs.3.rs-10404333/v1

License: This work is licensed under a Creative Commons Attribution 4.0 International License.
Read Full License

Additional Declarations: No competing interests reported.

Version of Record: A version of this preprint was published at BMC Genomics on September 10th, 2026. See the published version at https://doi.org/10.1186/s12864-026-13324-3.

Abstract

Background

The Tibetan brown bear (*Ursus arctos pruinosus*) is an apex predator endemic to the Qinghai-Xizang Plateau (QXP) with crucial ecological status, while high-quality genomic resources for studying its plateau-adaptated evolution remain scarce.

Results

Here, we generated a chromosome-level genome assembly of a female Tibetan brown bear from QXP, using PacBio HiFi and Hi-C sequencing. The final assembly spans 2.42 Gb, with scaffold N50 of 72.35 Mb, contig N50 of 66.56 Mb and GC content of 42.36%. Comparative genomic analyses revealed high chromosomal synteny between Tibetan brown bear and polar bear. Demographic reconstruction of Tibetan brown bear demonstrated an population expansion during the early Pleistocene, followed by two significant population bottlenecks at approximately 2 Mya (pre-Poyang Glaciation) and 0.1 Mya (the Last Glacial Period), leading to a cumulative effective population size reduce of nearly 80%. Notably, Tibetan brown bear hibernation-related pathway analyses revealed a specific carbohydrate-dominated metabolic strategy that differs strikingly from the lipid metabolism-dependent hibernation pattern of North American brown bear. This distinct metabolic adaptation highlights its unique adaptive mechanisms for surviving extreme QXP environments.

Conclusion

This high-quality genome assembly provides a valuable genomic resource for exploring the evolutionary history of ursidae and facilitates future conservation and management.

Introduction

Brown bear (*Ursus arctos*) is the most widely distributed extant large terrestrial carnivore [1]. Benefiting from abundant datasets covering its life history, demography, and phylogeography, this well-studied mammal serves as a model species for large carnivores research [2]. The brown bear exhibits a complex phylogeographic structure, with frequent topological incongruences among phylogenetic trees derived from mitochondrial DNA (mtDNA) and nuclear genome [3–5]. PSMC analyses have further revealed highly variable demographic histories across brown bear populations that the species experienced a global population decline since 1 Mya (Early Pleistocene) while the European and Gobi populations underwent a regional recovery during the last interglacial period [4–7]. In addition, previous studies have reported inconsistent divergence times between brown bear and its sister species, polar bear [5, 8–10].

Tibetan brown bear (*Ursus arctos pruinosus*) is a subspecies endemic to the Qinghai-Xizang Plateau (QXP [11]). Existing studies mainly focus on its ecological characristics, including activity pattern [12], human-bear conflict [13], and dietary [11, 14]. Molecular phylogenetic studies of this subspecies remain limited. Early researches using different molecular datasets revealed topological conflict: phylogenetic trees constructed from complete mitogenomes supported the Tibetan brown bear as sister lineage to the southern Hokkaido brown bear, whereas Cyt *b*-based phylogenies placed it as an independent lineage [15]. Subsequent studies have consistently recognized the Tibetan brown bear as an distinct evolutionary lineage [16, 17]. To date, high-quality genome data is still lacking, leaving the phylogenetic relationship of *U. a. pruinosus* ambiguous.

Hibernation is an adaptive survival strategy widely observed in mammals. By actively suppressing metabolic rate, body temperature and physiological activity, animals reduce energy consumption to survive cold winter with food scarcity [18–20]. Unlike common hibernating mammals such as rodents [21], bats [22], primates [23], ursidae [24] is the only group of large hibernating mammals [25]. In contrast to small hibernators who can lower body temperature to near-ambient level, bears experience only a moderate temperature reductiondecrease. This trait attributed to their large body mass, which helps maintain a stable core temperature [26]. Hibernation trait vary considerably across ursid species [25]. Three extant bear species—Asian black bear (*U. thibetanus*), American black bear (*U. americanus*), and brown bear (*U. arctos*)—hibernate during winter [24, 27]. The extinct cave bear (*U. spelaeus*) is also hypothesized to be a hibernator [28]. In contrast, other ursids, like giant panda (*Ailuropoda melanoleuca*), spectacled bear (*Tremarctos ornatus*), sloth bear (*Melursus ursinus*), and sun bear (*Helarctos malayanus*) do not exhibit the hibernation behaviour [25, 29, 30]. Polar bear shows sex-specific hibernation that males do not hibernate, while females retain partial hibernation-related adaptations [31, 32]. Even among hibernating bears, hibernation duration is modulated by multiple environmental factors, including latitude, temperature, food availability, and altitude [33, 34]. For instance, Asian black bears take a long hibertaion for 5–6 months in the Russian Far East [35], compared with merely 3 months in the Qinling Mountains of China [36]. Against this background, the Tibetan brown bear inhabits extreme high-altitude QTP, an environment characterized by intense ultraviolet radiation and hypoxia. It remains unclear whether this subspecies has evolved unique genetic adaptations in hibernation-associated pathways.

For the first time, we present a chromosome-level reference genome of the Tibetan brown bear, assembled using PacBio HiFi long-reads and Hi-C data. We further investigate its phylogenetic relationships and demographic history. By integrating enrichment analyses, we identify candidate genes and pathways potentially under positive selection during hibernation adaptation. This genomic resource provides a valuable foundation for exploring high-altitude adaptation, conducting mammalian comparative genomics, and advancing conservation straitegies for this QXP flagship carnivore.

Results

Tibetan brown bear genome assembly and assessment

For Tibetan brown bear, a total of 607.44 Gb of raw sequencing data was generated, comprising 130.93 Gb of PacBio HiFi long-reads and 161.78 Gb (~ 54X) Illumina paired-ended short reads, and 314.73 Gb of Hi-C data (Table 1). An estimated genome size of 1.91 ~ 2.01 Gb, with a heterozygosity rate of 0.43 ~ 1.55% (Fig. 1A).

Table 1
Statistics of sequencing data.

Sequencing Method	Total bases (bp)	Sequence coverge (×)
Illumina	161,777,814,300	66.8
PacBio	130,925,200,792	54.1
Hi-C	314,731,514,510	130
Total	607,434,529,602	-

After meticulously correcting sequencing errors and assembling the sequences, we obtained approximately 2.42 Gb genome assembly for the Tibetan brown bear, exhibiting high continuity with scaffold N50 of 72.35 Mb, contig N50 of 66.56 Mb and GC content of 42.36% (Fig. 1B, Table 2). Only 14 gaps were present across the entire assembly, with a cumulative gap length of 1,400 bp. Moreover, 37 chromosome pairs (2n = 74) were successfully clustered using Hi-C data, achieving an attachment rate of 97.55% (Fig. 1C and Table S2).

Table 2
Summary statistics of Tibetan brown bear (U. a. pruinosus) genome assembly.

Feature	Value
Assembly genome length (bp)	2,419,545,236
GC (%)	42.36
Contigs number	149
Contig N50 (Mb)	66.56
Contig N90 (Mb)	28.18
Longest contig (Mb)	110.62
Scaffolds number	135
Scaffold N50 (Mb)	72.35
Scaffold N90 (Mb)	37.88
Longest scaffold (Mb)	124.77
Number of chromosomes	37

A chromosome-level genome assembly was successfully achieved, with 59 telomeres and 25 centromeres detected in total. 25 of 37 chromosomes had telomeres repeated at both ends, and 9 chromosomes had telomeres at only one end, while chr33, chr35, and chr36 had none (Fig. 2, Table S1). A total of 99.8% of BUSCOs were identified (Table 3), with a k-mer completeness of 96.63% and a genome quality value (QV) of 47.24, indicating high genome completeness.

Table 3
BUSCO predictive statistics (vertebrata_odb9).

Categories	Genes number	Percentage %
Complete BUSCOs	3346	99.8
Complete and single-copy BUSCOs	3329	99.3
Complete and duplicated BUSCOs	17	0.5
Fragmented BUSCOs	2	0.1
Missing BUSCOs	6	0.2
Total vertebrata_odb9 BUSCO groups searched	3354	-

Gene annotation

Specifically, we identified 585,117 simple sequence repeats (SSRs) spanning 14,289,826 bp (0.59% of genome, Table S4), and 593,865 tandem repeats covering 128,069,142 bp (5.29% of genome, Table S5). Transposable elements (TEs) accounted for 43.65% of the genome, dominated by long interspersed elements (LINEs, 27.17%), short interspersed elements (SINEs, 9.15%), and long terminal repeats (LTRs, 5.65%) (Fig. 3, Table S3).

A total of 22,579 protein-coding genes were predicted with an average gene length of 44,200.49 bp. These genes contained an average of 9.51 exons per gene. The mean lengths of exon and intron were 324.51 bp and 4,533.02 bp. The average length of coding sequence (CDS) was 1,613.45 bp. Additionally, we identified 121,159 non-coding RNA genes, including 843 rRNA, 115,956 tRNA, and 1,536 miRNA genes (Table 4). 22,002 protein-coding genes were successfully assigned functional classifications through comparative analysis against multiple reference databases (Table 5, Table S6 and S7). This high annotation rate of 97.49% demonstrated comprehensive functional characterization of the genome assembly. Length distribution of genes were comparable to those of the related Ursidae (Fig. 4, Table S8). Genome completeness was evaluated using BUSCO, which detected approximately 97.44% of 14502 complete BUSCOs, and confirmed a high reliability of the gene annotation (Table 6).

Table 4
Non-coding RNA (ncRNA) annotation statistics.

Type	Number	Average Length (bp)	Total Length (bp)	Base Ratio (%)
28S rRNA	127	5,010	636,388	0.0263
18S rRNA	114	1,713	195,306	0.0081
5.8S rRNA	51	152	7,795	0.0003
5S rRNA	551	144	63,014	0.0026
tRNA	115,956	81	9,488,085	0.3921
miRNA	1,536	77	118,327	0.0049
snoRNA	650	113	73,515	0.003
catalytic RNA	10	244	2,445	0.0001
spliceosomal RNA	1,253	112	141,582	0.0059
other snRNA	5	61	306	0
lncRNA	183	145	26,661	0.0011
cis regulator	288	69	20,046	0.0008
other ncRNA	435	261	113,945	0.0047

Table 5
Gene functional annotation statistics.

Database	Number	Ratio(%)
COG/KOG	21,011	93.1
KEGG	215,315	67.86
GO	17,076	75.66
Pfam	20,344	90.14
NR	21,957	97.29
Swiss-Prot	20,568	91.13
TrEMBL	21,695	96.13
Overall	22,002	97.49
Query	22,569	100

Table 6
Quality assessment of annotated genes in Tibetan brown bear (U. a. pruinosus).

Type	Number	Percent (%)
Complete BUSCOs (C)	14,131	97.44
Complete and single-copy BUSCOs (S)	13,789	95.08
Complete and duplicated BUSCOs (D)	342	2.36
Fragmented BUSCOs (F)	83	0.57
Missing BUSCOs (M)	288	1.99
Total BUSCO groups searched	14,502	100.00

Synteny analysis

The chromosomes of Tibetan brown bear (*U. a. pruinosus*) exhibit a one-to-one correspondence with those of its closest relative, *U. maritimus*, with reverse sequences present on some chromosomes (Fig. 5).

Phylogenetic reconstruction of the mitochondrial genome

In the phylogenetic tree constructed based on mitochondrial genomes, YS061 and YS062, ZD13 and 91204, ZD05 and 91503 shared an identical haplotype, removed sample YS062, 91204 and 91503, other eight brown bear samples from Qinghai (YS061, ZD01, ZD05, ZD11, ZD13, 91602, 91702, TJ20) were clustered into a single clade together with the samples of Tibetan brown bear from Xizang (AP012592), which supports their conspecific membership in the Tibetan brown bear. This clade was clearly separated from brown bear subspecies of other geographic origins (e.g., Siberia, Northern Europe, North America), indicating the genetic independence and geographical specificity of Tibetan brown bear (Fig. 6).

(A) Maximum likelihood (ML) phylogeny. Samples shown in bold represent those used in this study. Numbers along branches represent bootstrap support values. (B) Divergence time tree estimated based on fossil evidence. The diagram labels the major mitochondrial DNA lineages and their geographic regions. The numbers at the nodes indicate the mean age in million years ago (Mya). Terminal taxa are designated by sample codes or previously reported accession numbers. The blue bars at the nodes represent the 95% highest posterior density (HPD) intervals of the node age estimates. The circles at the nodes indicate fossil calibration points. The horizontal axis at the bottom represents relative divergence time (in millions of years ago, relative scale).

Demographic history

Based on the PSMC analysis of all individuals, the effective population size (*Ne*) of *U. a. pruinosus* showed an initial increase during the Early Pleistocene, followed by a decline around ~ 2 Mya and a subsequent period of stabilization. Afterward, *Ne* dropped again approximately ~ 0.1 Mya, reaching an extremely low level and remaining stable thereafter, with a total significant drop by nearly 80% (Fig. 7).

PSMC results showed the demographic history of *U. a. pruinosus*, with a generation time (g) of 10 years and a mutation rate (μ) of 0.84×10^{-8} per site per generation. The time axis is logarithmically transformed.

Identification and functional annotation of hibernation genes

KEGG pathway enrichment analysis indicated that the Tibetan brown bear (YS061) was significantly enriched in the pathway of glycolysis/gluconeogenesis ($-\log_{10}$ FDR q = 8.9) and oxidative phosphorylation ($-\log_{10}$ FDR q = 4.0), in which the North American brown bear showed no enrichment (Fig. 8A). Tibetan brown bear also had a weak enrichment in the necroptosis pathway ($-\log_{10}$ FDR q = 2.0). In contrast, the North American brown bear showed enrichment in pathways of autophagy ($-\log_{10}$ FDR q = 5.4), AMPK signaling ($-\log_{10}$ FDR q = 5.3), adipocytokine signaling ($-\log_{10}$ FDR q = 5.3), insulin resistance ($-\log_{10}$ FDR q = 3.4), insulin signaling ($-\log_{10}$ FDR q = 2.3), PPAR signaling ($-\log_{10}$ FDR q = 2.4) and glucagon signaling ($-\log_{10}$ FDR q = 1.6), in which no enrichment detected in Tibetan brown bear.

GO functional enrichment analysis (Fig. 8B) further revealed subspecies-specific enrichment in Tibetan brown bear, including gluconeogenesis ($-\log_{10}$ FDR q = 6.0), glycolytic process ($-\log_{10}$ FDR q = 5.3), energy derivation by oxidation of organic compounds ($-\log_{10}$ FDR q = 1.8), mitochondrial membrane ($-\log_{10}$ FDR q = 4.2), mitochondrial translation ($-\log_{10}$ FDR q = 4.2), small molecule metabolic process ($-\log_{10}$ FDR q = 4.6), cellular respiration ($-\log_{10}$ FDR q = 5.0), ATP metabolic process ($-\log_{10}$ FDR q = 9.7), response to stimulus ($-\log_{10}$ FDR q = 10.8), obsolete oxidation-reduction process ($-\log_{10}$ FDR q = 5.4) and homeostatic process ($-\log_{10}$ FDR q = 1.7). In contrast, the North American brown bear only displayed weak enrichment in muscle contraction ($-\log_{10}$ FDR q = 3.5) and steroid hormone receptor signaling pathway ($-\log_{10}$ FDR q = 2.2).

(A) Heatmap showing the enrichment significance of KEGG pathways associated with hibernation. The color scale represents $-\log_{10}$ (FDR q-value), where higher values (darker red) indicate stronger statistical significance. (B) Heatmap of selected GO terms related to hibernation, Values are $-\log_{10}$ (FDR q-value). Deeper green indicates greater enrichment, while white or light color denotes non-significant enrichment.

Discussion

We assembled the first high-quality, near-T2T chromosome-level genome of the Tibetan brown bear (*Ursus arctos pruinosus*), which constitutes a valuable genetic resource for evolutionary studies of large carnivores. The assembled genome size is 2.42 Gb, with a GC content of 42.36%, a QV of 47.24, a k-mer completeness of 96.63% and a BUSCO completeness of 99.8%. Compared to the published chromosome-level genome of the North American brown bear (*U. a. horribilis*) [6], our near-T2T assembly harbors only 14 gaps across 37 chromosomes, exhibits longer scaffold N50 (+ 2.25 Mb) and contig N50 (+ 22.66 Mb), contains 43.34 Mb less repetitive sequences, and identifies 2,099 more annotated functional protain-coding genes. The brown bear (*Ursus arctos*) and the polar bear (*Ursus maritimus*) share a close phylogenetic relationship as members of the family Ursidae. Their genomes exhibit high synteny and share a stable karyotype of 2n = 74 [37, 38], further supporting the high-quality of our assembly. Compared with the synteny analysis of the North American brown bear and polar bear reported previously [6], our work provides clearer delineation of homologous genomic regions and establishes unambiguous one-to-one chromosome orthologous with higher resolution.

Phylogenetic results supports the Tibetan brown bear as a distinct evolutionary lineage. Its divergence from other brown bear populations around 2.27 Mya, probably driven by long-term geographic isolation and adaptive evolution under plateau conditions. Additionally, the divergence time between polar bear and brown bear at approximately 1 Mya, estimated in this study, is consistent with previous findings [39, 40].

PSMC analyses reveals that the Tibetan brown bear experienced a similar demographic trajectory to other brown bear subspecies [4, 41], with its drastic historical population fluctuations closely related to the Pleistocene climatic oscillations and the tectonic uplift of the QXP. Early Pleistocene population expansion of Tibetan brown bear was presumably facilitated by relatively warmer and less extreme environmental conditions, a biogeographic pattern consistent with that of the Asian black bear, which was restricted to southern glacial refugia during the Early Pleistocene and expanded northward only during the Middle Pleistocene [42]. This expansion scenario is also consistent with the demographic dynamics of other large mammals endemic to the QTP, such as the wild yak (*Bos mutus*) [43]. The subsequent population decline at approximately 2 Mya, corresponding to the Biber Glaciation, (the pre-Poyang Glaciation in China [44]), coincides with the beginning of the Middle Pleistocene transition, a notable climatic shift marked by prolonged and intensified glacial cycles [45]. These dramatic climatic changes substantially shrank suitable habitats and triggered population fragmentation. Notably, this demographic contraction corresponds exactly to the estimated divergence time (2.27 Mya) of the Tibetan brown bear. The significant population bottleneck of Tibetan brown bear during the Last Glacial Maximum (LGM) is not an isolated event. Phylogeographic evidence has documented pre-LGM distribution changes in Beringian brown bear populations [46]. Widespread glacial refugial retreats were also observed across multiple mammalian species during the LGM: European brown bears contracted to southern refugia [47], North American black bears retreated to southeastern refugia [48], and the giant pandas experienced severe population bottleneck due to glacial expansion and bamboo forest fragmentation [49]. The simultaneous population declines have likewise been identified in other QXP carnivores such as snow leopard (*Panthera uncia*) [50], further confirming that late Pleistocene extreme

climatic perturbations triggered broad-scale habitat fragmentation and resource scarcity, and imposing pervasive demographic constraints on plateau wildlife communities.

Significantly different from other ursid species, Tibetan brown bear exhibits hibernation-enriched pathways in the glycolysis/gluconeogenesis, oxidative phosphorylation, and necroptosis, whereas polar bear enriches the nitric oxide metabolic pathway and North American brown bear enriches the PPAR signaling pathway [51, 52]. We also identified significant enrichment of autophagy, AMPK signaling, adipocyte cytokine signaling, and insulin resistance pathway in North American brown bear, indicating the greater dependence on lipid metabolism and energy sensing mechanisms during hibernation, which is consistent with previous founding [52]. KEGG enrichment analysis of other QXP hibernating speceis, including high Himalaya frog (*Nanorana parkeri*) and Daurian ground squirrel (*Spermophilus dauricus*), also show the pentose phosphate pathway and glycolysis enrichment during hibernation [53, 54]. These consistent metabolic profiles demonstrate convergent hibernation adaptation across QXP endemic species, which primarily maintain overwintering metabolism stability via carbohydrate utilization. In this context, Tibetan brown bear may have evolved an unique hibernation energy strategy centered on carbohydrate utilization to cope with the extreme environment of hypoxia and low temperatures on the QXP.

In this study, we systematically presented the phylogenetic relationship, population history, and hibernation-related adaptive mechanisms of the Tibetan brown bear. Demographic reconstruction indicates that all of brown bear subspecies have experienced significant convergent population fluctuations and currently maintain relatively low effective population size (*Ne*). The specific enrichment of glycolysis/gluconeogenesis and oxidative phosphorylation pathways during hibernation of the Tibetan brown bear highlights its carbohydrate metabolism-dominated adaptive strategy, providing new insights into the molecular basis of adaptation in QXP mammals. Nevertheless, the evolutionary history underlying this adaptation remains unclear, necessitating further investigations with expanded samples and nuclear genomic data. Overall, this study deepens our understanding of brown bear phylogenetics and population dynamics, and provides valuable high-quality genomic resource for future researches on extreme high-altitude adaptation mechanisms and conservation genomics of plateau carnivores.

Materials and Methods

Sample collection

The 11 samples used in this study were obtained from Yushu Tibetan Autonomous Prefecture and Haixi Mongolian and Tibetan Autonomous Prefecture, Qinghai, China. Two blood samples (YS061 and YS062) were collected from two female brown bears injured in Xiewu town, and transferred from the anticoagulant tube to the cryogenic tube. Four muscle tissues (ZD01, ZD05, ZD11, ZD13) were obtained from Lancang River Source Management Committee of Sanjiangyuan National Park Administration and four muscle tissues (91204, 91503, 91602, 91702) were obtained from in Zadoi county. And one muscle tissues (TJ20) were obtained from in Tianjun county. All samples were transported in a liquid nitrogen

container (-180°C) and stored in an ultra-cold storage freezer at -80℃ in the College of Life Sciences, Qinghai Normal University. All the methods were carried out in accordance with the Code of Practice for the Care and Handling of animal guidelines.

DNA extraction and sequencing

The genome sequencing was performed on sample YS061, and the whole-genome resequencing on the other five samples. High-quality DNA was extracted using the Genomic DNA extraction kit (QIAGEN® Genomic). The degradation and contamination status of the extracted DNA were detected by 0.75% agarose gel electrophoresis. Subsequently, the DNA purity was determined using a NanoDrop™ One ultramicro spectrophotometer (Thermo Fisher Scientific, USA), with acceptable OD260/280 ratios ranging from 1.8 to 2.0 and OD260/230 ratios between 2.0 and 2.2. Finally, a Qubit® 3.0 Fluorometer (Invitrogen, USA) was employed for accurate quantification of DNA concentration.

After ensuring the DNA quality, the DNA was randomly fragmented using g-TUBEs (Covaris, USA). Target DNA fragments were enriched and purified using magnetic bead-based selection. The fragmented DNA was subjected to comprehensive damage repair and end-repair, and then connect stem-loop adapters sequences at both ends. Failed ligation products were subsequently removed through exonuclease digestion. Precise size selection was performed using the BluePippin system (Sage Science, USA), followed by library purification. Quality assessment of the library fragment size distribution was conducted using an Agilent 2100 Bioanalyzer (Agilent Technologies, USA). For PacBio SMRTbell library construction, hairpin adapters were ligated to generate circular templates. The prepared library was then subjected to single-molecule real-time (SMRT) sequencing on the Revio platform, where optimal template: enzyme complexes were loaded into zero-mode waveguides (ZMWs).

After sequencing, raw data processing involved removal of low-quality reads and adapter sequences to generate subreads. Circular Consensus Sequencing (CCS) analysis was performed to generate high-fidelity (HiFi) reads (Q20 threshold) through multiple alignment and error correction of subreads derived from individual template molecules. In parallel, quality-approved libraries were sequenced on MGI platforms using paired-end 150 bp (PE150) chemistry to generate complementary short-read data. To ensure the reliability of sequencing data, we first performed filtering processing on the raw data obtained from NGS paired-end sequencing using the fastp v0.21.0 preprocessing software (with default parameters) to remove low-quality reads, adapter sequences, and reads containing poly-N [55]. All of the sequencing services were provided by the Haorui Genomics Technology Co., Ltd., (Xi'an, China).

Genome survey and assembly

Genome size and heterozygosity were estimated by the kmer analysis using NGS DNA data prior [56]. The genome K-mer completeness and quality value (QV) was evaluated based on Illumina data using Merqury (v1.3) [57]. The workflow is as follows: For the cleaned data, 17-mer frequency distribution analysis was performed on sequence files using jellyfish v2.3.0 [58] and KMC v3.1.1 [59]. Subsequently, findGSE [60] and GenomeScope 2.0 [61] were used to estimate the genome size based on the 17-mer depth distribution derived from the cleaned sequencing reads of the 350-bp library, employing the

formula G = K-num/K-depth (where K-num represents the total number of 17-mers, K-depth denotes the k-mer depth, and G stands for the genome size). Further combining the simulation data results of Drosophilidae with different heterozygosity and the frequency peak distribution of 17 kmer, the heterozygosity and repeat content of Tibetan brown bear genome were estimated.

The high-quality HiFi reads was used for primary assembly by hifiasm v0.19.9 [62], with default parameters. To evaluate the accuracy of the assembly, all the MGI paired end reads were mapped to the assembled genome using BWA (Burrows-Wheeler Aligner) [63] and the mapping rate and genome coverage of sequencing reads were assessed using SAMtools [64]. Besides, base accuracy of the assembly was calculated with bcftools [64].

Hi-C reads were aligned to the draft assembly using BWA. The chromosome-level scaffolding were performed using HapHiC [65] with default parameters. The initial assembly and scaffolding files were visually error-corrected using JuiceBox v2.13.07 [66] software, with corrections made via heatmaps [67]. Telomeres in the assembly were detected with repetitive sequences (TTAGGG) as queries, using quarTeT (v1.2.2) [68]. Centromeric regions were delineated using Centromics v0.3 based on HiFi and HiC data. The completeness of the genome assembly was evaluated using BUSCO v5.0 [69] with the vertebrate database.

Genome annotation

Simple Sequence Repeats (SSR) motifs were identified using Krait v1.4.0 [70], while tandem repeats were detected with Tandem Repeats Finder v4.09 (TRF) [71]. Dispersed repetitive elements were annotated using RepeatMasker v4.1.2 [72]. Following quality control, clean RNA-seq reads were aligned to the reference genome using HISAT2 v2.2.1 [73], and transcripts were assembled with StringTie v2.2.1 [74]. Gene structures were predicted by merging transcript assemblies across all samples. For homology-based prediction, protein sequences from five Ursidae species, including *Ailuropoda melanoleuca* (GCF_002007445.2, GCF_000004335.2), *Ursus americanus* (GCF_020975775.1), *Ursus arctos* (GCF_023065955.2), and *Ursus maritimus* (GCF_017311325.1), were aligned to the genome using GeneMark-ETP v1.00 [75], ProtHint v2.6.0 [76], and Spaln v2.4.13f [77]. De novo gene prediction was performed with Augustus v3.4.0 [78], and all evidence was integrated into a consensus gene set using TSEBRA v1.1.1 [79]. The weighting scheme for evidence sources using barker3 v3.0.8 configured as follows: protein homology (P) weight = 1, RNA-seq assembly (E) weight = 20, EST (C) and cDNA (M) weights = 1. The minimum intron support fraction was set to 0.2, while start/stop codons required full support (fraction = 1). Allowable error margins for various features were also defined (e_1 = 0.1, e_2 = 0.5, e_3 = 0.05, e_4 = 0.2). This weighted integration strategy significantly improved the accuracy of gene models, particularly for alternatively spliced transcripts. Non-coding RNAs were predicted by comparing assembled sequences to the Rfam database with Infernal v1.1.4 [80]. And tRNA genes were annotated using tRNAscan-SE v1.23 [81] with default eukaryotic parameters. Functional annotation of protein-coding genes was conducted against public databases, including Non-Redundant (NR), Kyoto Encyclopedia of Genes and Genomes (KEGG), Eukaryotic Orthologous Groups of protein (KOG), gene ontology (GO), Swiss-Prot and TRanslation of EMBL (TrEMBL). Using BUSCO v5.2.2 to evaluate the

predicted gene set, assess the gene content of the existing sequences in the transcriptome, and thereby evaluate the completeness of the predicted gene set.

Synteny analysis

The high accuracy and continuity of *U. a. pruinosus* genome assembly were validated through direct comparison of chromosomal structures at the genomic level. Pairwise syntenic blocks between *U. a. pruinosus* and *U. maritimus* were identified using the JCVI v1.5.11 [82].

Phylogenetic reconstruction of the mitochondrial genome

We extracted the mitochondrial genome sequences from all the eleven genomic data using the GetOrganelle [83] software package. For our eleven samples, the sequences were aligned using the MUSCLE algorithm within MEGA 12 [84]. The resulting alignment in FASTA format was then imported into DnaSP v6 [85] to identify haplotypes. Redundant samples sharing identical haplotypes were subsequently removed from the dataset. To construct the phylogenetic tree, we downloaded mitochondrial genomes from other brown bear subspecies as the ingroup and seven other Ursidae species, *Canis lupus* and *Phoca largha* as the outgroup (Table S1). Multiple sequence alignment of the mitochondrial genome sequences of all samples was performed using the MUSCLE algorithm implemented in MEGA 12. Based on the aligned sequences, phylogenetic trees were constructed using the Maximum Likelihood (ML) methods. We used fossil evidence and previously reported divergence times from the literature as calibration points to estimate species divergence times. First, we queried the TimeTree database and obtained three optimal fossil calibration points, which were used as prior information. Then, the aligned mitochondrial sequence data (NEXUS file) were imported into BEAUti 2 to set the substitution model, molecular clock model, and prior distributions for the calibration nodes, generating an .xml file. The generated log file was then imported into Tracer v1.7.2 [86] to check for acceptable mixing and convergence to the stationary distribution. The .xml file was imported into BEAST v2.7.7 [87] for Bayesian MCMC analysis. After the run was completed, the resulting .trees file was imported into TreeAnnotator to generate a maximum clade credibility (MCC) tree. Finally, the MCC tree file was imported into FigTree v1.4.5 [86] for visualization and graphical adjustment.

Demographic history

All eleven genome data obtained in this study were used to reconstruct the historical demographic trajectory of *U. a. pruinosus*. The Pairwise Sequentially Markovian Coalescent (PSMC) model [88] was applied to estimate the effective population size (N) of *U. a. pruinosus*. We set a generation time of 10 years and mutation rate $\mu = 0.84\times10^{-8}$ mutations/site/year [89].

Identification and functional annotation of hibernation genes

To investigate the functional divergence and ecological adaptations among bear species, we conducted GO term enrichment and KEGG pathway enrichment analyses by integrating our genomic data with North American brown bear. Enrichment was assessed using Fisher's exact test, with the background gene set defined as the union of all genes from the two species. To correct for multiple testing, we applied the

Benjamini-Hochberg false discovery rate (FDR) [90], and adjusted P-values (q-values) < 0.05 were considered statistically significant. Enrichment strength is visualized in heatmaps and bar plots as $-\log_{10}$ (q - value).

Declarations

Ethics approval and consent to participate

Permission for field surveys, sample collection and experiments was granted by the Qinghai Normal University, China (Approval No. 2026-14).

Consent for publication

Not applicable.

Data Availability Statement

The DNA sequencing data have been deposited into the China National GeneBank DataBase (CNGBdb, https://db.cngb.org) with the project accession number CNP0008053 and CNP0009490, and sequencing ID of CNR1425799, CNA0733069, CNR1555542 and CNR1555543.

All software and pipelines were executed according to the methods section. No custom code was generated for this study.

Competing interests

The authors declare that they have no competing interests.

Funding

This work was supported by the National Natural Science Foundation of China (Grant No. 32360133 and 32560252).

Author Contributions

Guogang Li and Nan Sun conceived and designed the study. Chenxing Yu and Yanlin Liu collected the samples. Muran Zhao and Anmin Wang performed the bioinformatics analysis. Hai Liu performed data checking and uploading. The manuscript is written by Muran Zhao and revised by Guogang Li and Nan Sun. All authors read and approved the final manuscript for submission.

Acknowledgements

We thank all the field assistants and collaborators involved in the Tibetan brown bear sampling and lab work.

References

1. Naeem S, Haider J, Younus M, et al. Status and distribution of Himalayan brown bear. Deosai National Park and its buffer valleys, gilgit-baltistan (Survey Report 2022)[R]. Gilgit-Baltistan, Pakistan: Forest, Wildlife and Parks Department; 2022.
2. Davison J, Ho SYW, Bray SC, et al. Late-quaternary biogeographic scenarios for the brown bear (*Ursus arctos*), a wild mammal model species[J]. Q Sci Rev. 2011;30:418–30.
3. de Jong MJ, Niamir A, Wolf M, et al. Range-wide whole-genome resequencing of the brown bear reveals drivers of intraspecies divergence[J]. Commun Biology. 2023;6:153.
4. Tumendemberel O, Hendricks SA, Hohenlohe PA, et al. Range-wide evolutionary relationships and historical demography of brown bears (*Ursus arctos*) revealed by whole-genome sequencing of isolated central Asian populations[J]. Mol Ecol. 2023;32:5156–69.
5. Miller W, Schuster SC, Welch AJ et al. Polar and brown bear genomes reveal ancient admixture and demographic footprints of past climate change. Proceedings of the National Academy of Sciences, 2012, 109: E2382-E2390.
6. Armstrong EE, Perry BW, Huang Y, et al. A beary good genome: haplotype-resolved, chromosome-level assembly of the brown bear (*Ursus arctos*)[J]. Volume 14. Genome Biology and Evolution; 2022. p. evac125.
7. Endo Y, Osada N, Mano T, et al. Demographic history of the brown bear (*Ursus arctos*) on Hokkaido Island, Japan, based on whole-genomic sequence analysis[J]. Genome Biol Evol. 2021;13:evab195.
8. Kurtén B. The evolution of the polar bear, *Ursus maritimus Phipps*[J]. Acta Zool Fennica. 1964;108:1–30.
9. Hailer F, Kutschera V, Hallström B, et al. Nuclear genomic sequences reveal that polar bears are an old and distinct bear lineage[J]. Science. 2012;336:344–7.
10. Lindqvist C, Schuster SC, Sun Y, et al. Complete mitochondrial genome of a Pleistocene jawbone unveils the origin of polar bear[J]. Proc Natl Acad Sci USA. 2010;107:5053–7.
11. Xu A, Jiang Z, Li C, et al. Food habits and hunting patterns of Tibetan brown bear during warm seasons in Kekexili region on Qinghai-Tibetan Plateau[J]. Zoological Res. 2010;31:670–4.
12. Chen X, Li Y, Xie P, et al. Suitable habitat and daily activity patterns of Ursus arctos pruinosus in Dulan County, Qinghai Province[J]. Acta Theriol Sinica. 2024;44:321–32.
13. Dawaciren. Hazards and preventive measures of human-wildlife conflict in the Qiangtang region[J]. China Tibetol. 2010;4:71–8.
14. Cong W, Zhang Y, Huang TF, et al. Dietary composition and niche partitioning of sympatric carnivores in Altun Mountain National Nature Reserve[J]. Acta Theriol Sinica. 2024;44:695–705.
15. Matsuhashi T, Masuda R, Mano T, et al. Phylogenetic relationships among worldwide populations of the brown bear *Ursus arctos*[J]. Zoolog Sci. 2001;18:1137–43.
16. Hirata D, Mano T, Abramov AV, et al. Molecular phylogeography of the brown bear (*Ursus arctos*) in Northeastern Asia based on analyses of complete mitochondrial DNA sequences[J]. Mol Biol Evol.

2013;30:1644–52.
17. Lan T, Gill S, Bellemain E et al. Evolutionary history of enigmatic bears in theTibetan Plateau-Himalaya region and the identity of the yeti[J]. Proceedings of the Royal Society B: Biological Sciences, 2017, 284:20171804.
18. Robbins CT, Lopez-Alfaro C, Rode KD, et al. Hibernation and seasonal fastingin bears: the energetic costs and consequences for polar bears[J]. J Mammal. 2012;93:1493–503.
19. Carey HV, Andrews MT, Martin SL. Mammalian hibernation: cellular and molecular responses to depressed metabolism and low temperature[J]. Physiol Rev. 2003;83:1153–81.
20. Geiser F. Metabolic Rate and Body Temperature Reduction During Hibernation and Daily Torpor[J]. Annual Rev Physiol. 2004;66:239–74.
21. Kisser B, Goodwin HT. Hibernation and overwinter body temperatures in free-ranging thirteen-lined ground squirrels, Ictidomys tridecemlineatus[J]. Am Midl Nat. 2012;167:396–409.
22. Rauch JC, Beatty DD. Comparison of regional blood distribution in *Eptesicus fuscus* (big brown bat) during torpor (summer), hibernation (winter), and arousal[J]. Can J Zool. 1975;53:207–14.
23. Dausmann KH, Glos J, Ganzhorn JU, et al. Hibernation in a tropical primate[J]. Nature. 2004;429:825–26.
24. Nelson RA. Winter sleep in the black bear. A physiologic and metabolic marvel[J]. Mayo Clinic Proceedings, 1973, 48: 733–737.
25. Perry BW, Jansen HT, Enstrom AN, et al. Genomic insights into bear hibernation[J]. Annu Rev Genet. 2025;59:147–64.
26. Evans AL, Fuchs B, Singh NJ, et al. Body mass is associated with hibernation length, body temperature, and heart rate in free-ranging brown bears[J]. Front Zool. 2023;20:27.
27. Nelson RA, Folk GE, Pfeiffer EW, et al. Behavior, biochemistry, and hibernation in black, grizzly, and polar bears[J]. Bears: Their Biology Manage. 1983;5:284–90.
28. Hofreiter M, Paijmans JLA, Goodchild H, et al. The future of ancient DNA: Technical advances and conceptual shifts[J]. BioEssays. 2015;37:284–93.
29. Bi W, Hou R, Owens JR, et al. Field metabolic rates of giant pandas reveal energetic adaptations[J]. Sci Rep. 2021;11:22391.
30. Laurie A, Seidensticker J. Behavioural ecology of the sloth bear (*Melursus ursinus*)[J]. J Zool. 1977;182:187–204.
31. Pagano AM, Durner GM, Rode KD, et al. High-energy, high-fat lifestyle challenges an Arctic apex predator, the polar bear[J]. Science. 2018;359:568–72.
32. Pagano AM, Rode KD, Lunn NJ, et al. Polar bear energetic and behavioral strategies on land with implications for surviving the ice-free period[J]. Nat Commun. 2024;15:947.
33. Evans AL, Singh NJ, Friebe A, et al. Drivers of hibernation in the brown bear[J]. Front Zool. 2016;13:7.
34. González-Bernardo E, Russo LF, Valderrábano E, et al. Denning in brown bears. Ecol Evol. 2020;10:6844–62.

35. Kolchin S, Oleynikov A, Volkova E et al. Activity patterns of the Asiatic black bear in the Russian Far East based on camera-trap data[J]. Ursus, 2025, 2025: 1–16.
36. Zahoor B, Liu X, Wu P, et al. Activity pattern study of Asiatic black bear (*Ursus thibetanus*) in the Qinling Mountains, China, by using infrared camera traps[J]. Volume 28. Environmental Science and Pollution Research; 2021. pp. 25179–86.
37. Nash WG, Wienberg J, Ferguson-Smith MA, et al. Comparative genomics: tracking chromosome evolution in the family ursidae using reciprocal chromosome painting[J]. Cytogenet Cell Genet. 1998;83:182–92.
38. Nash WG, O'Brien SJ. A comparative chromosome banding analysis of the Ursidae and their relationship to other carnivores[J]. Cytogenet Cell Genet. 1987;45:206–12.
39. Kumar V, Lammers F, Bidon T, et al. The evolutionary history of bears is characterized by gene flow across species[J]. Sci Rep. 2017;7:46487.
40. Zou TT, Kuang WM, Yin TT, et al. Uncovering the enigmatic evolution of bears in greater depth: The hybrid origin of the Asiatic black bear[J]. Proc Natl Acad Sci USA. 2022;119:e2120307119.
41. Lan T, Leppälä K, Tomlin C, et al. Insights into bear evolution from a Pleistocene polar bear genome[J]. Proc Natl Acad Sci USA. 2022;119:e2200016119.
42. Hu H, Tong H, Yu H, et al. New study sheds light on the impressive intraspecific variation of Quaternary Asiatic black bears in China[J]. Quatern Int. 2023;646:22–33.
43. Qiu Q, Wang LZ, Wang K, et al. Yak whole-genome resequencing reveals domestication signatures and prehistoric population expansions[J]. Nat Commun. 2015;6:10283.
44. Shi Y. Quaternary glaciation and environmental change in China[M]. Hebei Science and Technology Publishing House; 2006.
45. Clark PU, Archer D, Pollard D, et al. The middle Pleistocene transition: characteristics, mechanisms, and implications for long-term changes in atmospheric pCO_2[J]. Q Sci Rev. 2006;25:3150–84.
46. Barnes I, Matheus P, Shapiro B, et al. Dynamics of pleistocene population extinctions in beringian brown bears[J]. Science. 2002;295:2267–70.
47. Marciszak A, Wagner J, Kyselý R, et al. The late pleistocene history of the brown bear *Ursus arctos* Linnaeus, 1758 in the czech republic[J]. Radiocarbon. 2022;64:1–17.
48. Pedersen M, de Sanctis B, Saremi N, et al. Environmental Genomics of Late Pleistocene Black Bears and Giant Short-Faced Bears[J]. Curr Biol. 2021;31:2724–30.
49. Zhao S, Zheng P, Dong S, et al. Whole-genome sequencing of giant pandas provides insights into demographic history and local adaptation[J]. Nat Genet. 2013;45:67–71.
50. Yang L, Jin H, Yang Q, et al. Genomic evidence for low genetic diversity but purging of strong deleterious variants in snow leopards[J]. Genome Biol. 2025;26:94.
51. Welch AJ, Bedoya-Reina OC, Carretero-Paulet L, et al. Polar bears exhibit genome-wide signatures of bioenergetic adaptation to life in the arctic environment[J]. Genome Biol Evol. 2014;6:433–50.

52. Jansen HT, Trojahn S, Saxton MW, et al. Hibernation induces widespread transcriptional remodeling in metabolic tissues of the grizzly bear[J]. Commun Biology. 2019;2:336.
53. Niu Y, Chen Q, Storey KB, et al. Physiological ecology of winter hibernation by the high-altitude frog Nanorana parkeri[J]. Physiol Biochem Zool. 2022;95:201–11.
54. Yang Y, Hao Z, An N, et al. Integrated transcriptomics and metabolomics reveal protective effects on heart of hibernating Daurian ground squirrels[J]. J Cell Physiol. 2023;238:2724–48.
55. Chen S, Zhou Y, Chen Y, et al. fastp: an ultra-fast all-in-one FASTQ preprocessor[J]. Bioinformatics. 2018;34:i884–90.
56. Liu B, Shi Y, Yuan J, et al. Estimation of genomic characteristics by analyzing k-mer frequency in de novo genome projects[J]. arXiv: Genomics; 2013.
57. Rhie A, Walenz BP, Koren S, et al. Merqury: reference-free quality, completeness, and phasing assessment for genome assemblies[J]. Genome Biol. 2020;21:245.
58. Marçais G, Kingsford C. A fast, lock-free approach for efficient parallel counting of occurrences of k-mers[J]. Bioinformatics. 2011;27:764–70.
59. Kokot M, Dlugosz M, Deorowicz S. KMC 3: counting and manipulating k-mer statistics[J]. Bioinformatics. 2017;33:2759–61.
60. Sun H, Ding J, Piednoël M, et al. findGSE: estimating genome size variation within human and Arabidopsis using k-mer frequencies[J]. Bioinformatics. 2018;34:550–7.
61. Ranallo-Benavidez TR, Jaron KS, Schatz MC. GenomeScope 2.0 and Smudgeplot for reference-free profiling of polyploid genomes[J]. Nat Commun. 2020;11:1432.
62. Cheng H, Concepcion GT, Feng X, et al. Haplotype-resolved de novo assembly using phased assembly graphs with hifiasm[J]. Nat Methods. 2021;18:170–5.
63. Li H, Durbin R. Fast and accurate short read alignment with Burrows-Wheeler transform[J]. Bioinformatics. 2009;25:1754–60.
64. Danecek P, Bonfield JK, Liddle J, et al. Twelve years of SAMtools and BCFtools[J]. Gigascience. 2021;10:giab008.
65. Zeng X, Yi Z, Zhang X, et al. Chromosome-level scaffolding of haplotype-resolved assemblies using Hi-C data without reference genomes[J]. Nat Plants. 2024;10:1184–200.
66. Durand NC, Robinson JT, Shamim MS, et al. Juicebox provides a visualization system for Hi-C contact maps with unlimited zoom[J]. Cell Syst. 2016;3:99–101.
67. Wolff J, Rabbani L, Gilsbach R, et al. Galaxy HiCExplorer 3: a web server for reproducible Hi-C, capture Hi-C and single-cell Hi-C data analysis, quality control and visualization[J]. Nucleic Acids Res. 2020;48:W177–84.
68. Lin Y, Ye C, Li X, et al. quarTeT: A telomere-to-telomere toolkit for gap-free genome assembly and centromeric repeat identification[J]. Hortic Res. 2023;10:uhad127.
69. Simão FA, Waterhouse RM, Ioannidis P, et al. BUSCO: assessing genome assembly and annotation completeness with single-copy orthologs[J]. Bioinformatics. 2015;31:3210–2.

70. Du L, Zhang C, Liu Q, et al. Krait: an ultrafast tool for genome-wide survey of microsatellites and primer design[J]. Bioinformatics. 2018;34:681–3.
71. Benson G. Tandem repeats finder: a program to analyze DNA sequences[J]. Nucleic Acids Res. 1999;27:573–80.
72. Tarailo-Graovac M, Chen N. Using RepeatMasker to identify repetitive elements in genomic sequences. Curr Protoc Bioinformatics[J]. Current Protocols in Bioinformatics Chapter, 2009, 4:4.10.1–4.10.14.
73. Kim D, Paggi JM, Park C, et al. Graph-based genome alignment and genotyping with HISAT2 and HISAT-genotype[J]. Nat Biotechnol. 2019;37:907–15.
74. Kovaka S, Zimin AV, Pertea GM, et al. Transcriptome assembly from long-read RNA-seq alignments with StringTie2[J]. Genome Biol. 2019;20:278.
75. Brůna T, Lomsadze A, Borodovsky M. GeneMark-ETP: automatic gene finding in eukaryotic genomes in consistence with extrinsic data[J]. BioRxiv, 2023, 524024.
76. Brůna T, Lomsadze A, Borodovsky M. GeneMark-EP+: eukaryotic gene prediction with self-training in the space of genes and proteins[J]. NAR Genomics Bioinf. 2020;2:lqaa026.
77. Iwata H, Gotoh O. Benchmarking spliced alignment programs including Spaln2, an extended version of Spaln that incorporates additional species-specific features[J]. Nucleic Acids Res. 2012;40:e161.
78. Stanke M, Diekhans M, Baertsch R, et al. Using native and syntenically mapped cDNA alignments to improve de novo gene finding[J]. Bioinformatics. 2008;24:637–44.
79. Gabriel L, Hoff KJ, Brůna T, et al. TSEBRA: transcript selector for BRAKER[J]. BMC Bioinformatics. 2021;22:566.
80. Nawrocki EP, Eddy SR. Infernal 1.1: 100-fold faster RNA homology searches[J]. Bioinformatics. 2013;29:2933–5.
81. Lowe TM, Eddy SR. tRNAscan-SE: a program for improved detection of transfer RNA genes in genomic sequence[J]. Nucleic Acids Res. 1997;25:955–64.
82. Tang H, Krishnakumar V, Zeng X, et al. JCVI: A versatile toolkit for comparative genomics analysis[J]. Imeta. 2024;3:e211.
83. Jin JJ, Yu WB, Yang JB, et al. GetOrganelle: a fast and versatile toolkit for accurate de novo assembly of organelle genomes[J]. Genome Biol. 2020;21:241.
84. Kumar S, Stecher G, Suleski M, et al. MEGA12: molecular evolutionary genetic analysis version 12 for adaptive and green computing[J]. Mol Biol Evol. 2024;41:msae263.
85. Rozas J, Ferrer MA, Sánchez-DelBarrio JC, et al. DnaSP 6: DNA sequence polymorphism analysis of large data sets[J]. Mol Biol Evol. 2017;34:3299–302.
86. Rambaut A. Figtree ver 1.4.4. Institute of Evolutionary Biology. Edinburgh: University of Edinburgh; 2018.
87. Bouckaert R, Heled J, Kühnert D, et al. BEAST 2: A software platform for bayesian evolutionary analysis[J]. PLoS Comput Biol. 2014;10:e1003537.

88. Li H, Durbin R. Inference of human population history from individual whole genome sequences[J]. Nature. 2011;475:493–6.
89. Wang R, Peña-Garcia Y, Bibby MG, et al. Examining the effects of hibernation on germline mutation rates in grizzly bears[J]. Genome Biol Evol. 2022;14:evac148.
90. Benjamini Y, Hochberg Y. Controlling the false discovery rate: A practical and powerful approach to multiple testing[J]. J Roy Stat Soc: Ser B (Methodol). 1995;57:289–300.

Figures

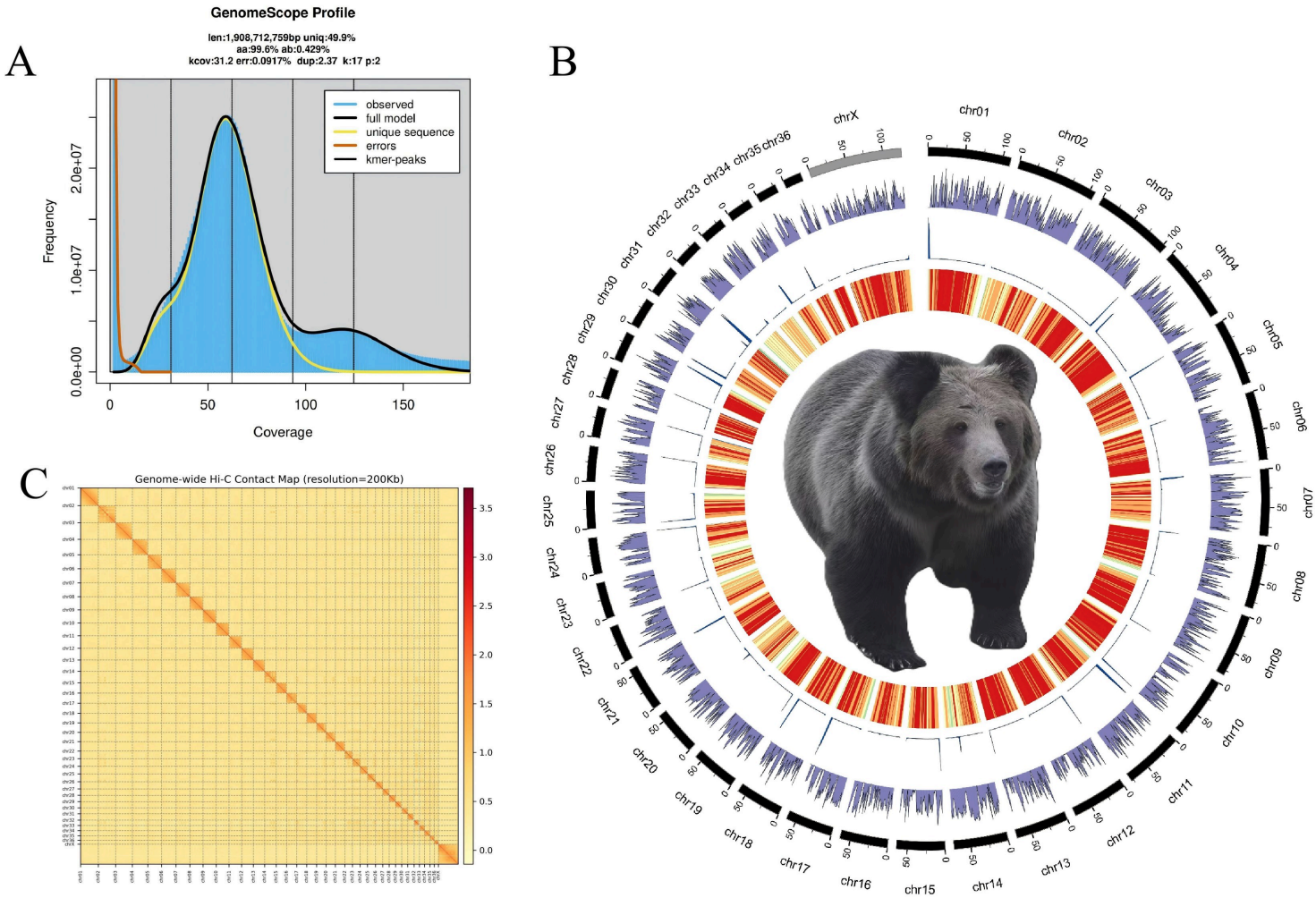

Figure 1

Genome analysis of Tibetan brown bear (*U. a. pruinosus*). **(A)** The k-mer frequency distribution for genome size estimation. **(B)** Circos plot of genome characteristics from outer to inner circles: chromosome length, gene density, repetitive sequence density, and GC content. **(C)** Hi-C intra-chromosomal contact map of genome assembly.

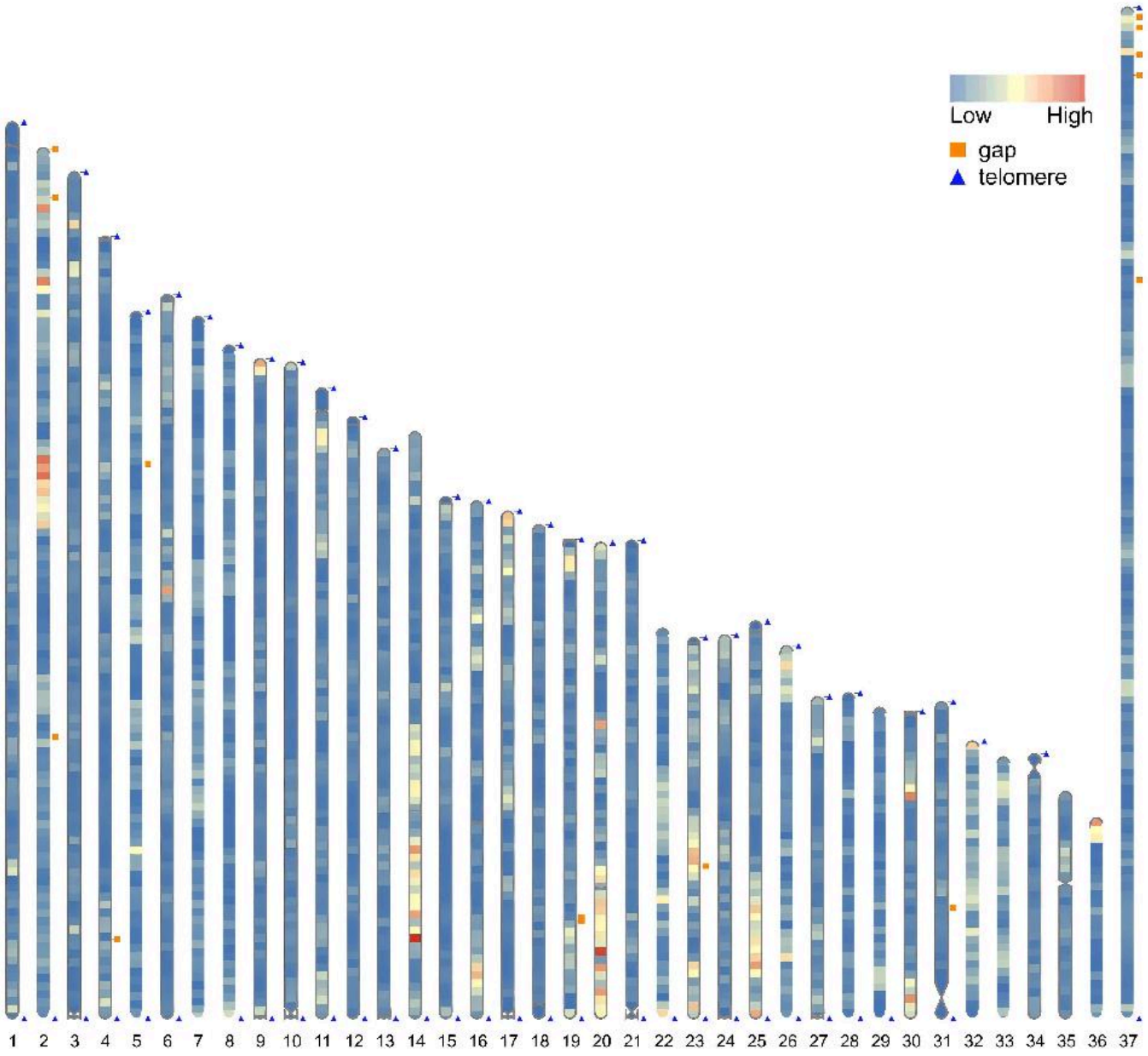

Figure 2

The schematic diagram of the 37 pairs of pseudo-chromosome sequences on Tibetan brown bear (*U. a. pruinosus*) genome. Low (blue) to high (red) gradual colors: repeats content in 50-kbp sliding windows. Orange square: the gaps between contigs. Blue triangle: telomere positions, characteristic structures at chromosome ends. The junction of the gray box: centromere positions.

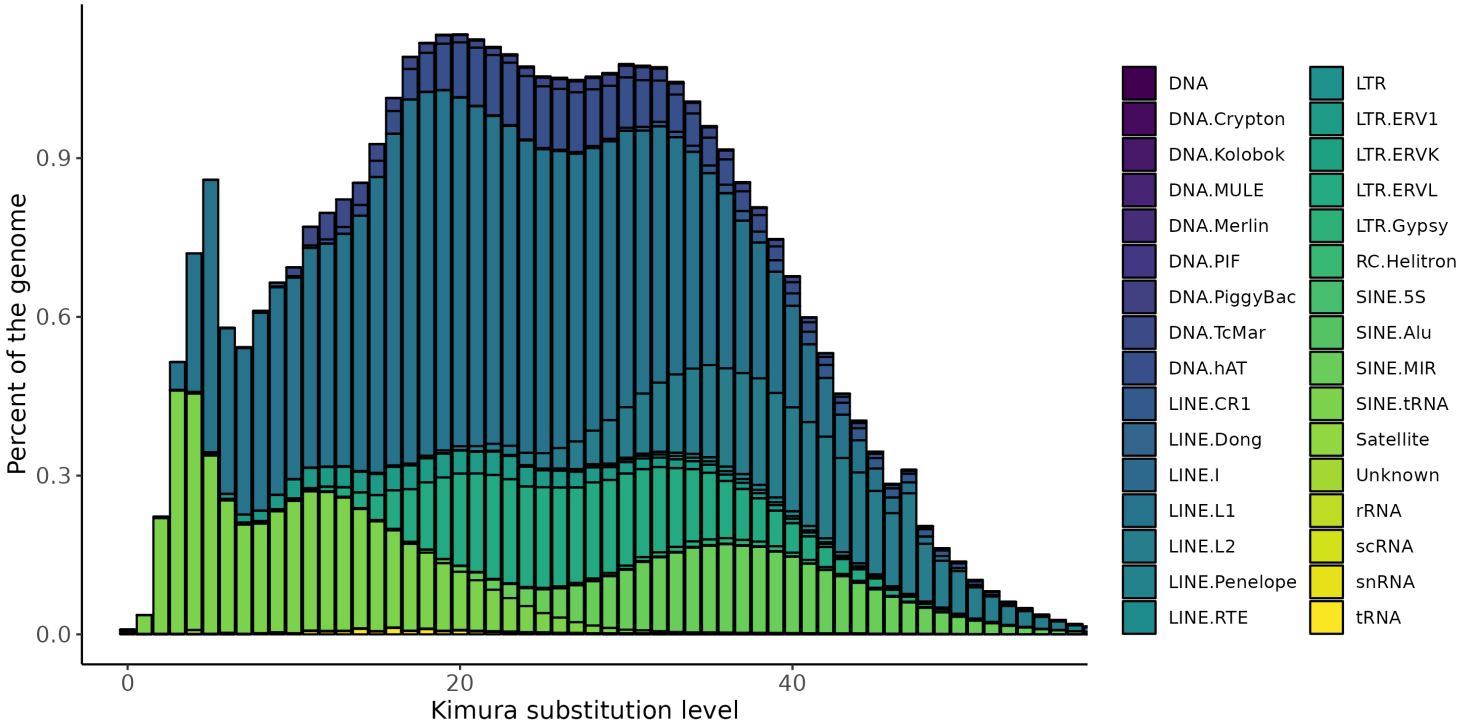

Figure 3

The Repetitive DNA Landscape in the Tibetan brown bear (*U. a. pruinosus*).

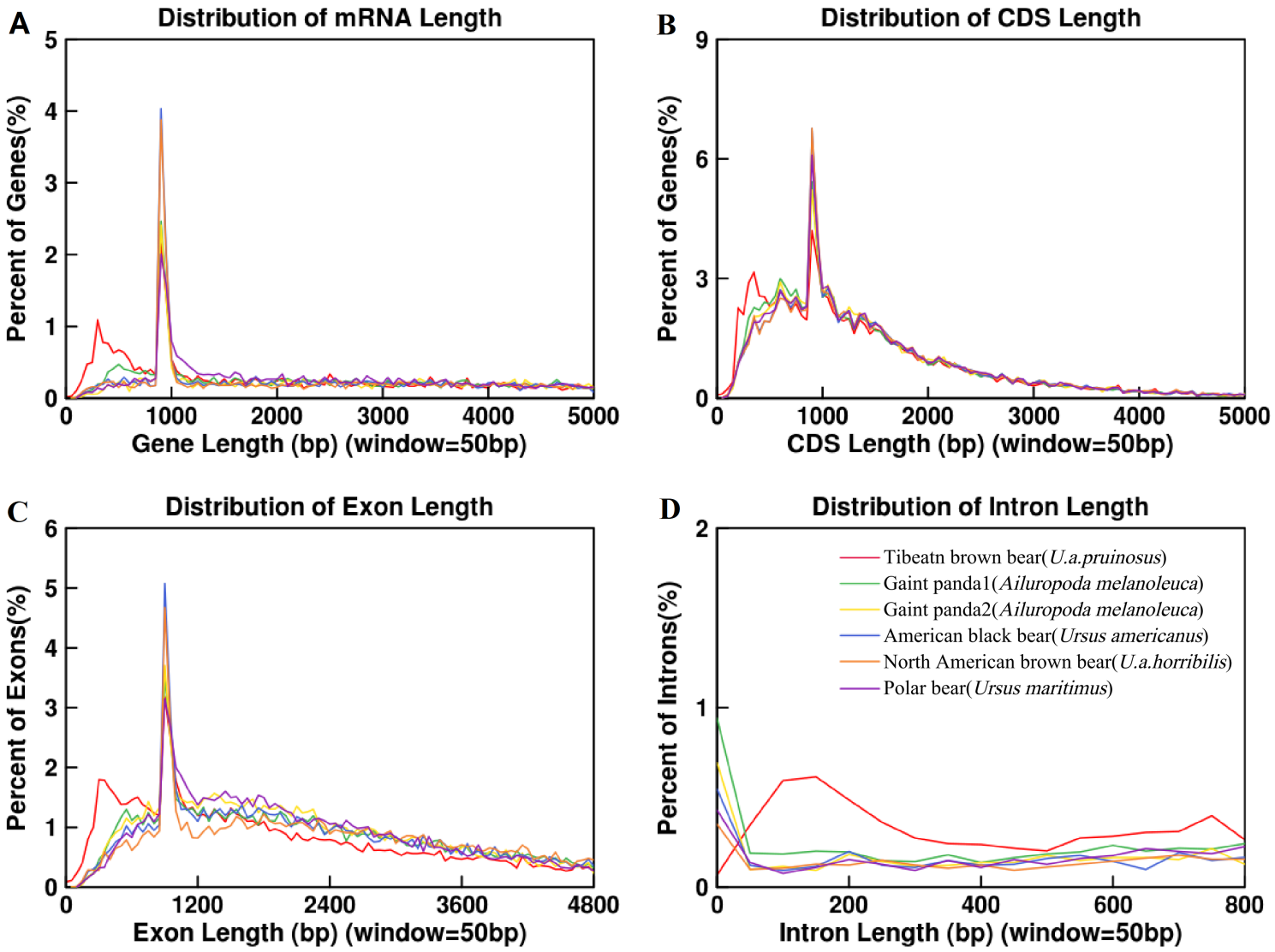

Figure 4

Length distribution comparison of (A) genes, (B) CDSs, (C) exons, and (D) introns for Tibetan brown bear (*U. a. pruinosus*) to those in the closely related Ursidae species.

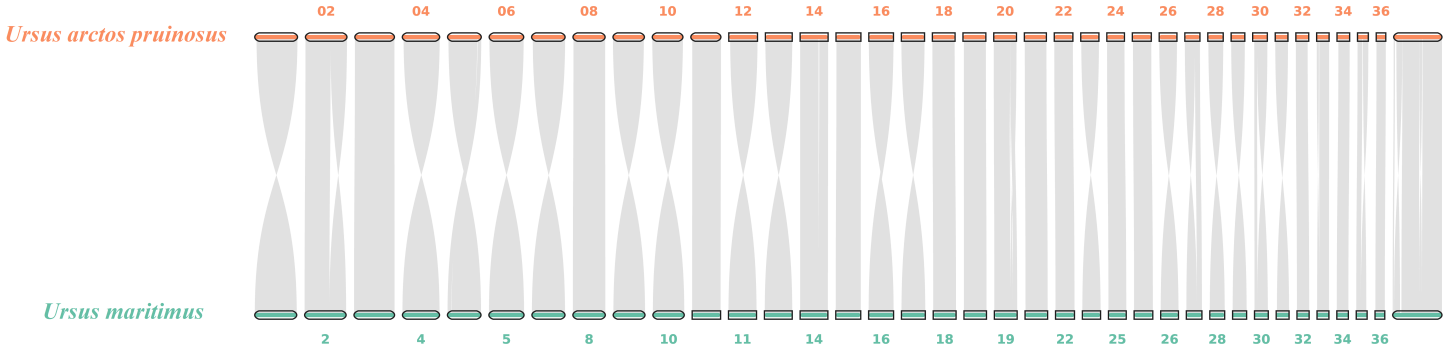

Figure 5

Collinear relationship of *U. a. pruinosus* and *U. maritimus*.

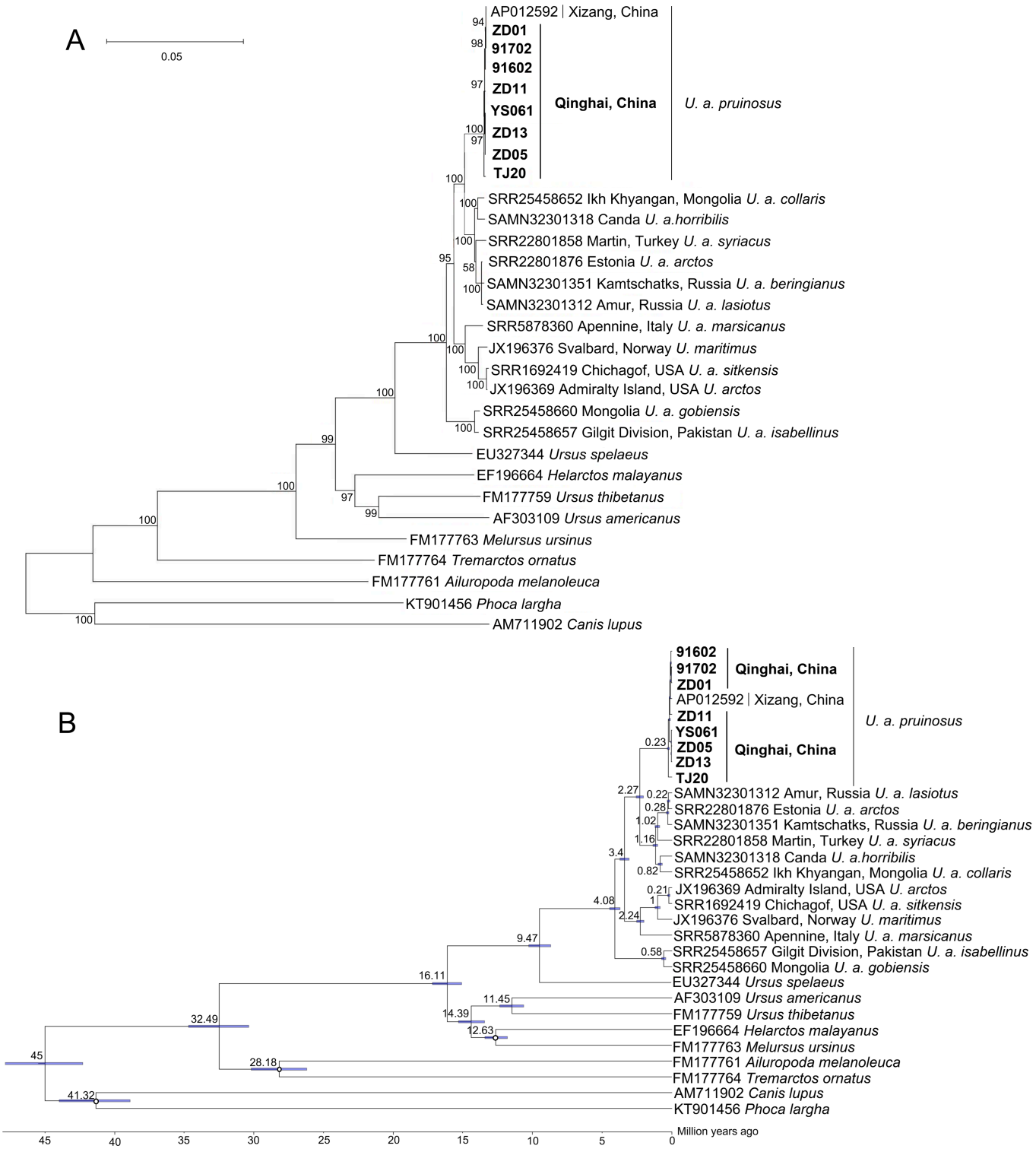

Figure 6

Phylogenetics of *U. a. pruinosus* at the mitochondrial genome level.

(A) Maximum likelihood (ML) phylogeny. Samples shown in bold represent those used in this study. Numbers along branches represent bootstrap support values. (B) Divergence time tree estimated based on fossil evidence. The diagram labels the major mitochondrial DNA lineages and their geographic

regions. The numbers at the nodes indicate the mean age in million years ago (Mya). Terminal taxa are designated by sample codes or previously reported accession numbers. The blue bars at the nodes represent the 95% highest posterior density (HPD) intervals of the node age estimates. The circles at the nodes indicate fossil calibration points. The horizontal axis at the bottom represents relative divergence time (in millions of years ago, relative scale).

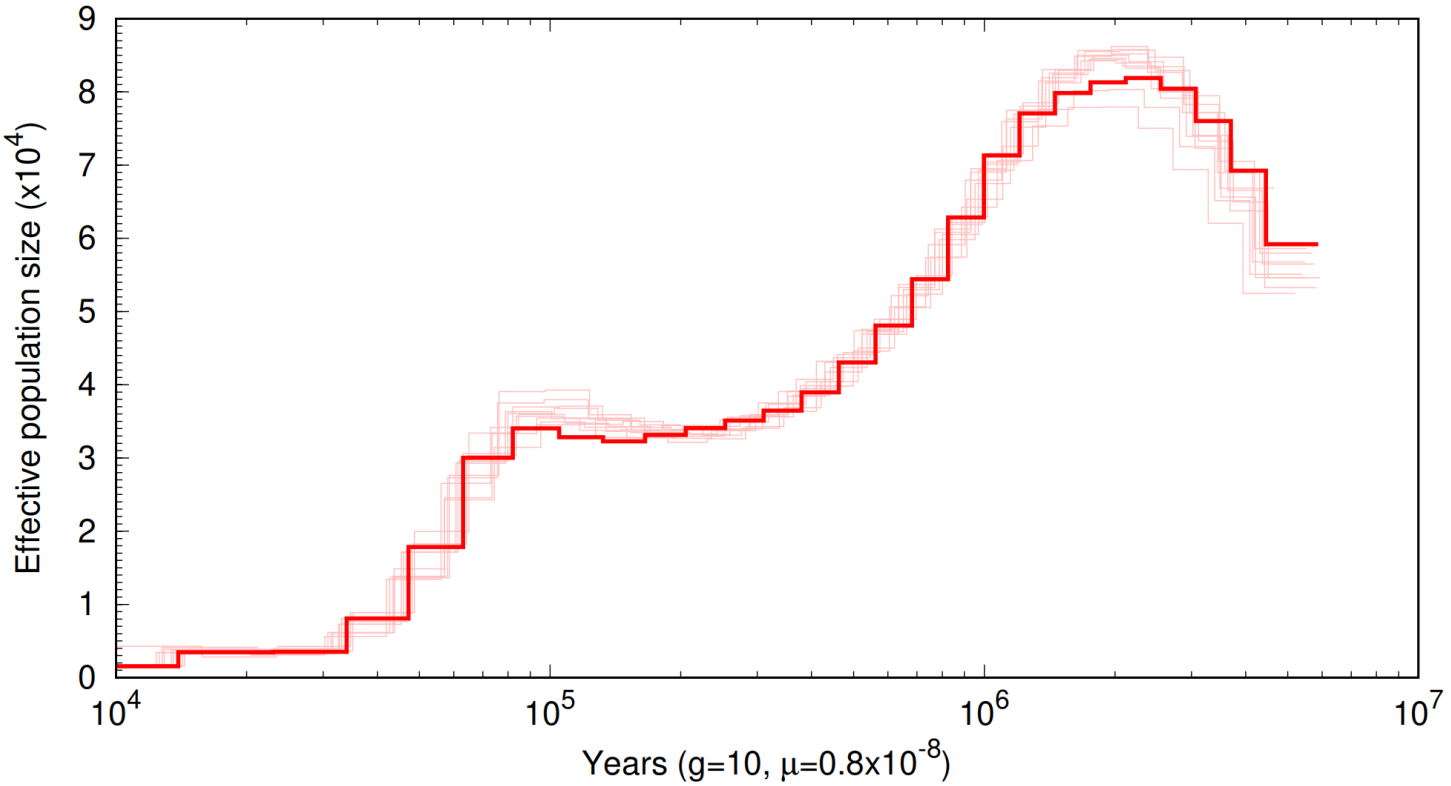

Figure 7

Demographic of *U. a. pruinosus*.

PSMC results showed the demographic history of *U. a. pruinosus*, with a generation time (g) of 10 years and a mutation rate (μ) of 0.84×10^{-8} per site per generation. The time axis is logarithmically transformed.

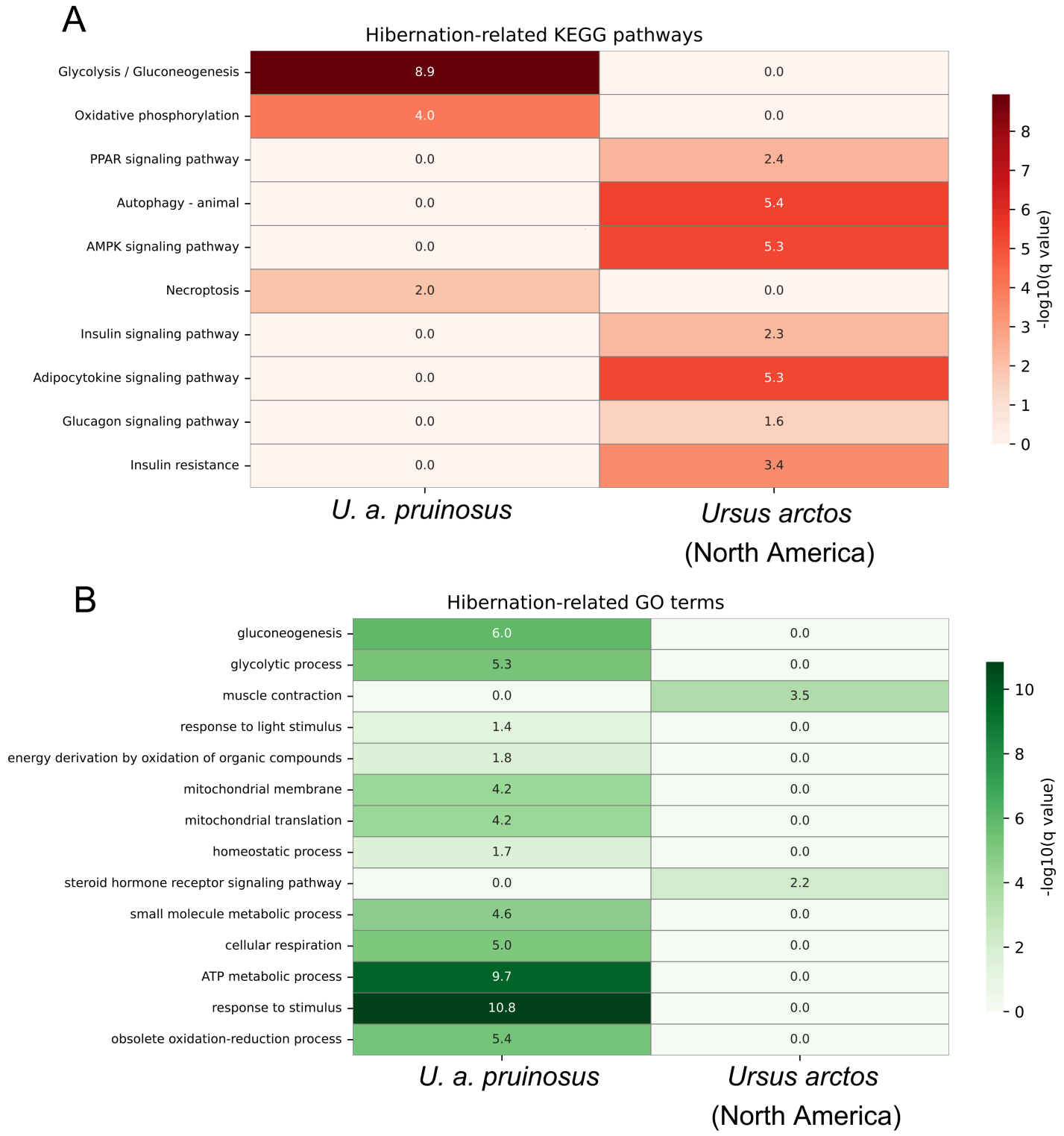

Figure 8

Comparative analysis of hibernation-related pathways in two bear species (Tibetan brown bear YS061 and North American brown bear) based on KEGG and GO enrichment.

(A) Heatmap showing the enrichment significance of KEGG pathways associated with hibernation. The color scale represents -$\log_{10}$ (FDR q-value), where higher values (darker red) indicate stronger statistical

significance. (B) Heatmap of selected GO terms related to hibernation, Values are -$\log_{10}$ (FDR q-value). Deeper green indicates greater enrichment, while white or light color denotes non-significant enrichment.

Supplementary Files

This is a list of supplementary files associated with this preprint. Click to download.

- GraphicalAbstractImage.jpg
- GraphicalAbstractText.doc
- SupplementaryMaterial.docx